Fibers and Polymers 2014, Vol.15, No.4, 744-752 DOI 10.1007/s12221-014-0744-4

Study on the Matrix-fibril Morphologies of Polypropylene/polystyrene Blends under Non-isothermal Uniaxial Elongational Flow

Houkang He†, Long Chen*†, Shanshan Sun, Tonghui Wang, Yu Zhang*, and Meifang Zhu

State Key Laboratory for Modification of Chemical Fibers and Polymer Materials, College of Material Science and Engineering, Donghua University, Shanghai 201620, P.R. China

(Received April 22, 2013; Revised September 7, 2013; Accepted September 18, 2013)

Abstract: Polypropylene/polystyrene blends with different viscosity ratios, p, ranging from 1.6×10^{-2} to 10.8, were prepared by using textile-grade isotactic polypropylene (iPP) and five kinds of atactic polystyrene (aPS), named PS1, PS2, PS3, PS31 and PS46 with different molecular weight, and then melt-spun into composite fibers with matrix-fibril morphology at different take-up velocities, v_L, ranging from 125 to 1000 m/min. The effects of p on the diameters and quantities of dispersed droplets in extrudate fibers, and the effects of p and v_L on the size and quantities of fibrils in take-up fibers were discussed, respectively. Based on a quantitatively characterization for the coalescence and deformation of droplets during melt spinning, a theoretical analysis based on Newtonian fluids simplification and the deformation theory was presented to predict the deformation and breakup of droplets during melt spinning. It is found that there is a good fit between theoretical and observed experimental results at most discussed take-up velocities. Furthermore, the uncertainties of Newtonian fluids simplification and a hypothesis of local energy dissipation from migration and coalescence were noted to explain the deviations between predicted and experimental data.

Keywords: Polypropylene/polystyrene, Deformation, Coalescence, Breakup, Melt spinning

Introduction

Polymer blending has been identified as one of the most versatile and economical method for producing new multiphase polymeric materials that are able to meet the demand for complex performance. Development of the multiphase polymer materials by blending is strongly dependent on the control of morphology. Matrix-fibril morphologies (MFMs) can be fabricated by the deformation of dispersed phases. Several parameters such as flow fields, capillary instability, deformation behaviors, coalescence, and interface properties have great impact on the MFM formation. Elongational and orientating flow fields are more effective than shear flow fields in transforming droplets into fibrous domains [1,2]. Recently, *in situ* reinforced polymer-polymer composites, so-called microfibrillar composites (MFCs), have been developed by fibrillation of the dispersed phase [3,4]. In the process, two immiscible thermoplastic polymers (TPs) are melt-blended. The MFCs are produced from the melt blends by a cold or hot drawing and a subsequent annealing of the drawn blends.

Modification of conventional TP fibers via the processing of compounding with another polymer and then melt spinning to fabricate MFM has been extensively investigated in recent decades. One of the most important processing is to blend a TP matrix with thermotropic liquid crystal polymers (TLCPs) to prepare the so-called '*in situ*' composite fibers with improved mechanical properties, especially elastic modulus and tensile strength [5-8]. TP/TP composite fibers with MFM, such as polyethylene terephthalate (PET)/ polypropylene (PP) [9], recycled PET/PP [10], PP/nylon 6 (N6) [11,12], to reinforce the matrix TPs also attracted widely attentions. Another important processing is modification of dyeability for conventional TP fiber. As a fiber material for clothing and household textiles, PP has light specific gravidity, good chemistry resistance, good heat and electrical insulation. But PP fibers are difficult to dye due to high crystallinity and the absence of dye sites in molecular chains. Some of TPs, such as N6 [13], PET [14], polybutylenes terephthalate (PBT) [15] and polystyrene (PS) [16,17], was selected to blend with PP to improve the dyeability of PP fibers. In addition, immiscible TP composite fibers with MFM have been also utilized to prepare ultrafine fibers in micro- or nanometer scaled size, by removing the matrix phase of the obtained composite fibers with suitable solvents in industry [18].

The properties of the composite fibers depend on the degree of deformation, the size, and the shape of the fibril phases. The formation of these fibril phases is primarily influenced by the melt spinning condition, that is, the properties of the composite fibers can be optimized by selecting suitable spinning condition. The main factors such as concentration of dispersed phases, viscosity ratios of the dispersed phases to the matrix phases, interfacial properties have been discussed. For example, Qin *et al.* [19-21] discussed the effects of TLCP concentration, condition of extrusion and drawing, and type of TLCP on the morphology of PP/ TLCP composite fibers. Takahashi *et al.* [22] reported the effect of viscosity ratios of the polymers on the morphology of PP/N6 composite fibers. Tavanaie *et al.* [15] obtained

†H He and L Chen contributed equally to this work.
*Corresponding author: happyjack@dhu.edu.cn
*Corresponding author: yzh@dhu.edu.cn

PBT fibrils with fine diameter when the viscosity ratio was less than 1 in PP/PBT composite fibers. Afshari *et al.* [23] found the size of N6 fibrils increased with an increase in the concentration of N6 in ternary composite fibers of PP, N6 and polymer compatibilizer.

Melt polymer flowing during non-isothermal melt spinning is a typical uniaxial elongational flow. However, there are few case reports of the modeling and prediction of the deformation and breakup of droplets under such flowing. Padsalgikar *et al.* [24] and Song *et al.* [25] simulated the deformation and breakup of dispersed phases during melt spinning process by simplifying the spinning fluid as a Newtonian fluid. Padsalgikar *et al.* predicted the deformation of PP droplets in PS matrix at take-up velocity under 350 m/min. Song *et al.* simulated the melt spinning of PET/TLCP and PBT/TLCP composite fibers at take-up velocity lower than 120 m/min, and found no breakup of the TLCP phase appeared. Unfortunately, it is always neglected about the coalescence of droplets during melt spinning. More recently, a scheme to describe the deformation and coalescence of droplets happened in spin line was presented by our group, resulting from the study of the fibril size and quantities and their distributions on cross sections of matrix fibers of PP/PS and low density polyethylene/N6 [26-28]. Nevertheless, no relevant numerical study or modeling on the deformation and coalescence has been carried out yet.

In this paper, five kinds of polypropylene/polystyrene blends were prepared by blending a textile-grade isotactic PP (iPP) and five kinds of atactic PS (aPS) with different molecular weight. The morphologies of the extrudate fibers collected in free-falling and take-up fibers at different velocities range from 125 to 1000 m/min was studied using scanning electron microscopy (SEM). The morphologies of selected fibers were characterized and discussed as a function of viscosity ratio and take-up velocity. The average elongational strain rate on the spin line was calculated based on steady-state melt spinning theory. For a primary theoretical consideration, we simplified the spinning fluid as a Newtonian fluid, and calculated the capillary number and the reduced capillary number based on definition equations for Newtonian systems. The deformation, breakup and coalescence of droplets during melt spinning were predicted based on capillary number theory.

Experimental

Materials

An iPP was supplied by Donghua University. Three raw materials of aPS with different molecular weight were used in this study. PS1 was purchased from BASF (trade name: Polystyrol 144C), PS2 was purchased from Taita Chemical Co., Ltd., Taiwan (trade name: 951F), and PS3 was supplied by Sigma-Aldrich (Product Number: 331651). Two blends of PS1 and PS2 were prepared through procedures described later. Main properties of raw materials were summarized in Table 1. All polymers were dried at 80 °C over night under vacuum to minimize the moisture contents prior to any use.

A Spurr's embedding kit, including vinyl cyclohexene dioxide (ERL-4221), diglycidyl ether of polypropylene glycol (DER 736), nonenyl succinic anhydride (NSA) and dimethylamino ethanol (DMAE), was product of Structure Probe, Inc., USA (trade name: SPI-Chem), and used as received. Tetrahydrofuran (THF) and ethanol were analytical reagent grade used as received.

Melt Blending

PS1 and PS2 were mixed at ratio of PS1/PS2 3:1 (PS31) and 4:6 (PS46) in weight by hand. Mixed materials were melt-blended at 230 °C by a HAAKE RC90 torque rheometer (Thermo Scientific, Germany) equipped with a twin-screw and an internal mixer.

Five polymer-pairs were mixed at ratio of iPP/aPS 92:8 in weight by hand. Mixed materials were melt blended by a twin-screw extruder (D=25 mm, L/D=35, screw velocity= 140 rpm) at 210 °C. Compounded strands were quenched by water, and then pelletized into 2×2 mm pellets.

Melt Spinning

Five polymer blends of iPP/aPS were melt spun on a lab-scale melt spinner with a single-screw extruder (D=25 mm,

Table 1. Main properties of raw materials of iPP and aPS with different viscosity ratios

Raw material		Melt flow rate[a] (g/10 min)	$T_{m,on\text{-}set}$ [b] (°C)	$T_{m,peak}$ [b] (°C)	M_w [c] (×10^5 g/mol)	M_w/M_n [c]	η_0 at 220 °C (Pa s)	$\eta_{0,aPS}/\eta_{0,iPP}$ at 220 °C
iPP		46.0	135.0	165.0	2.33	4.24	215.7	-
aPS	PS1	7.9	-	-	1.86	1.60	2321.3	10.8
	PS31	20.4	-	-	1.78	1.63	1097.0	5.1
	PS46	28.0	-	-	1.66	1.72	824.5	3.8
	PS2	45.0	-	-	1.55	1.81	328.1	1.5
	PS3	>45.0	-	-	0.35 [d]	-	3.48	1.6×10^{-2}

[a]Melt flow rate of iPP was measured at 230 °C/2.16 kg, and that of aPS was measured at 200 °C/5.00 kg, [b]measured by a 204F1 differential scanning calorimetry (NETZSCH, Germany), scanning from 25 °C to 250 °C at 10 °C/min, [c]measured by a gel permeation chromatography (Waters, USA), except PS3, and [d]data from supplier.

L/*D*=28, screw speed was controlled automatically to maintain the head pressure at 7±0.2 MPa), and a spinneret containing 36 orifices, each of 0.30 mm diameter and 0.25 *L*/*D*. The extruder was set as three different temperature zones, 200, 210, and 220 °C, at the feeding, compressing and metering sections, respectively. Metering gear-pump, melt pipe and spinneret were maintained at 220 °C. The volume flow rate of melts was 27 cm^3/min. The distance from spinneret to the first guide roller was about 1.5 m. The take-up fibers were air-quenched with cross air velocity of about 0.1 m/s at room temperature, and collected at the take-up velocity of 125, 250, 375, 500, 750, 1000 m/min. The extrudate fibers were collected when molten fibers were spun out and cooled immediately in a water bath set beneath the spinneret.

Rheological Measurement

An advanced rheometric expansion system (ARES, TA Instruments Inc., USA) was used in the steady mode with parallel plate fixtures to measure the viscosities of each component polymers of the composite fibers at 190 to 230 °C with an interval of 10 °C. Prior to tests, all polymer samples were compression molded to make 2.0 mm thick and 25 mm diameter discs by a hydraulic hot press that was set to 170 °C. The ARES was equipped with a Forced Convection Oven (FCO) - a platinum resistance thermometer sensor positioned at the center of the lower plate, and double 25 mm diameter parallel plates. For each test, the FCO was pre-heated to 160 °C, and then the polymer discs were loaded in between two parallel plates. Temperature was maintained at 160 °C for 4 min to melt the polymers; then it was set to test temperature and equilibrated for another 2 min prior to the rheological measurements. Steady sweeps were performed with shear rate ranging from 10^{-2} to 10^2 s^{-1}. All rheological measurements were repeated three times to demonstrate reproducibility.

SEM

Samples of multi-filaments were combed smoothly and embedded in Spurr's epoxy resin, thermo-set at 70 °C for 8 h. Spurr's epoxy resin was selected as suggested B-formula according to reference [29] to obtain appropriate hardness and hence high quality of sliced sections and SEM micrographs. A Leica RM2126 RT rotary microtome (Leica Microsystems, Germany) was used to slice the embedded fibers to obtain the cross and longitudinal sections. The sliced specimens were immersed into THF for 10 min at room temperature to etch the dispersed aPS domains, and then successively washed by ethanol and distilled water three times, with aid of ultrasonic wave, to remove the dissolved aPS. Dried specimens were golden coated, observed and photographed by a S-3000N SEM microscopy (Hitachi, Japan).

Image Analysis

The SEM micrographs on cross sections were evaluated with image analysis software Image-Pro Plus 6.0 (Media Cybernetics). Image analysis was automated, converting the micrographs into image displaying black droplets of aPS on gray background (matrix iPP), and in the second step routinely measuring position and equivalent diameter (*ED*) and quantity (*n*) of aPS droplets. *ED* was a size feature determining the diameter of a circle with the same area as the corresponding object. $\overline{ED}$ and $\overline{n}$ were the averages of equivalent diameters and quantities of droplets. For each experiment, five cross section views were analyzed and averaged arithmetically.

Results and Discussion

Rheological Properties and Viscosity Ratios

Since the deformation and coalescence of droplets dispersed in matrix are decided by two dimensionless parameters — capillary number *Ca* and viscosity ratio *p*, rheological properties of component polymers play a critical role to decide the morphologies of melt-spun composite fibers. The uniaxial elongational viscosity can be roughly estimated by $\eta_T=3\eta_0$, which is so-called as the Trouton's rule [30]. The zero shear viscosities η_0 of the component polymers were inferred from Carreau's model which expressed as below [31]:

$$\eta = \frac{\eta_0}{[1+(\lambda\dot{\gamma})^2]^{(1-n)/2}} \tag{1}$$

where η was the shear viscosity, λ the relaxation time, *n* the power-law exponent. The inferred η_0 at 220 °C were summarized in Table 1.

The viscosity in the temperature above the melting point was assumed to be approximated by the Arrhenius equation with activation energy ΔE_a:

$$\eta = A\exp\left(\frac{\Delta E_a}{RT}\right) \tag{2}$$

where *A* was intrinsic viscosity, *R* the Boltzmann constant, and *T* the absolute temperature. The ratio, *p*, of the viscosity of the droplet, η_d, to that of the matrix, η_m, was expressed as an Arrhenius-type equation as below:

$$p = (A_d/A_m)\exp\left(\frac{\Delta E_{a,d}-\Delta E_{a,m}}{RT}\right) \tag{3}$$

where the subscripts *d* and *m* was the droplet and the matrix respectively.

The viscosity ratios of different aPS to iPP at various temperatures were plotted in Figure 1. It was found that viscosity ratios increased when temperature decreased in all polymer pairs. This experimental relationship between viscosity ratios and temperatures was adopted for further discussion of the mechanism of formation of MFM.

Morphologies of iPP/aPS Extrudate Fibers

Morphologies of iPP/aPS extrudate fibers were shown in Figure 2. From the cross and longitudinal section views of

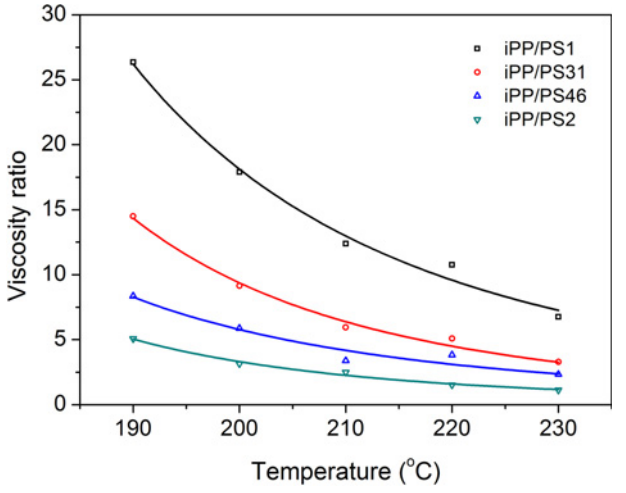

Figure 1. Viscosity ratios of different aPS to iPP as functions of temperature.

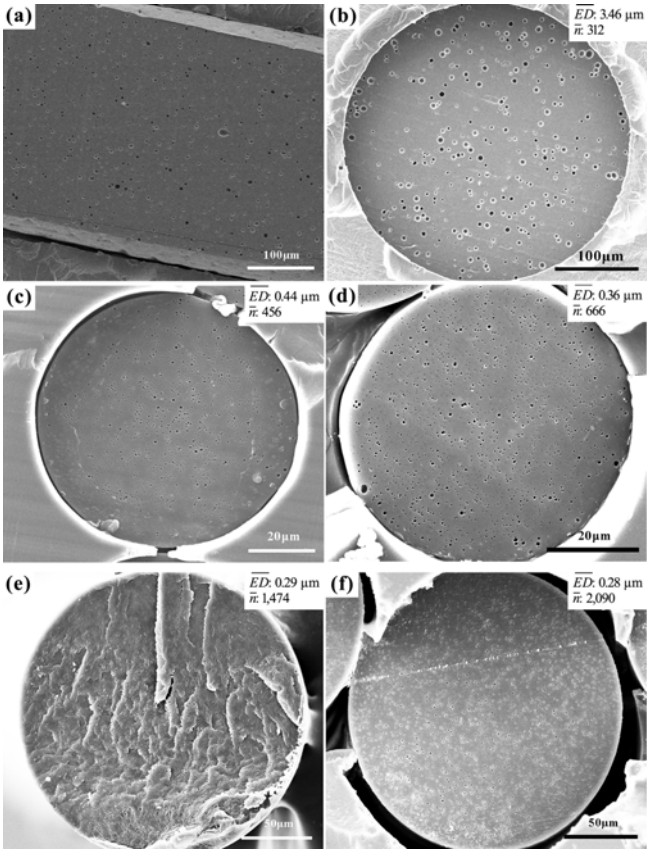

Figure 2. SEM micrographs of iPP/aPS extrudate fibers; (a) longitudinal section of iPP/PS1 and cross sections of (b) iPP/PS1, (c) iPP/PS31, (d) iPP/PS46, (e) iPP/PS2, and (f) iPP/PS3.

iPP/aPS (Figure 2(a), (b)), dispersed phases were shown as similar to spheres. Spherical droplets were formed after melts exit from the spinneret when the elastic energy was

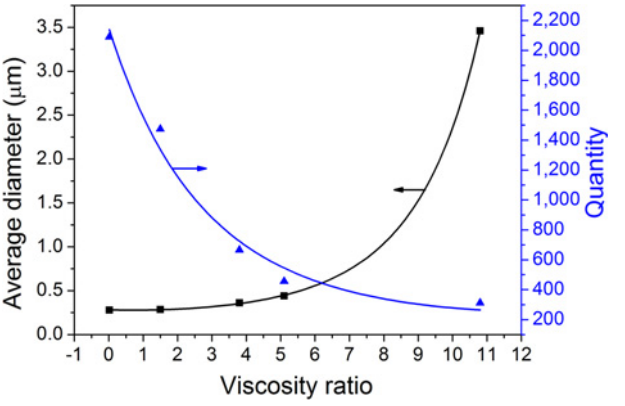

Figure 3. The average diameters and quantities of droplets in extrudate fibers as functions of viscosity ratio.

relaxed completely. Moreover, droplets were distributed uniformly on the cross section of extrudate fibers, which implied that homogeneous morphology was formed after elastic energy relaxation beneath the spinneret. As the viscosity of dispersed aPS increased, the viscosity ratio of droplets to matrixes increased, and the average diameters of aPS droplets increased exponentially, while the quantities of aPS droplets decreased exponentially, as shown in Figure 3. A lower viscosity ratio led to smaller droplets divided during shear flow in the orifices of the spinneret. And there were a critical droplet diameter and quantity at a certain shear rate. To obtain a finer morphology of extrudate, an increase of shear rate will be needed.

Morphologies of iPP/aPS Take-up Fibers

Longitudinal section view of dispersed phases in fiber taken at 500 m/min was shown in Figure 4. It was found that droplets were extended to fibrils in various lengths. This implied that comparing with the interfacial stress, the elongation viscous stress was in a leading role during melt spinning, and this unbalance promoted droplets to deform from spheres to ellipsoids. Moreover, the distribution in fibril length means either uneven deformation or breakup or coalescence of droplets occurred during melt spinning.

Cross section views of take-up fibers were shown in Figure 5 and Figure 6. The average equivalent diameters $\overline{ED}$ and quantities $\bar{n}$ of fibrils obtained from image analysis were shown in Table 2. We defined a coalescence ratio C to describe the reduction of the quantity of fibrils during melt spinning:

$$C = \frac{\bar{n}_{Ex}}{\bar{n}_{v_L}} \tag{4}$$

where the subscripts Ex and v_L were quantities of fibrils in extrudate fibers and take-up fibers respectively. If $C>1$, quantity of fibril reduced in take-up fibers with comparing to that of extrudate fibers and coalescence occurred. Whereas, if $C<1$, broken-up of fibril occurred.

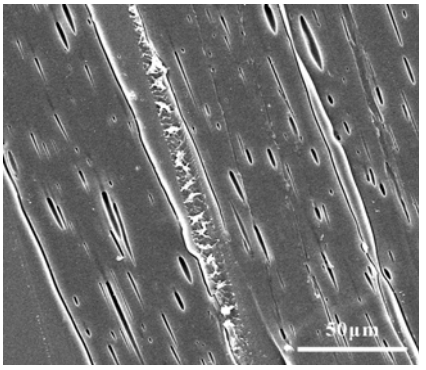

Figure 4. SEM micrograph of iPP/PS1 take-up fiber on longitudinal section.

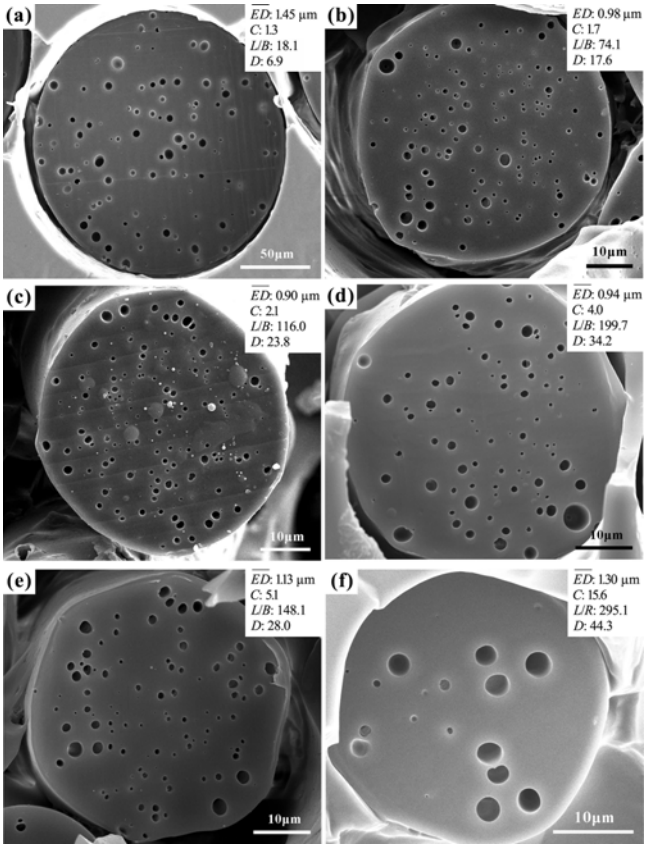

Figure 5. SEM micrographs of iPP/PS1 take-up fibers at various velocities; (a) 125, (b) 250, (c) 375, (d) 500, (e) 750, and (f) 1000 m/min.

The ratio *L/B* of fibrils on cross section view was decided by equation (5) based on a constant total volume of droplets during the melt spinning:

$$L/B = C\left(\frac{\overline{ED}_{Ex}}{\overline{ED}_{v_L}}\right)^3 \tag{5}$$

and the deformation ratio *D* was given by:

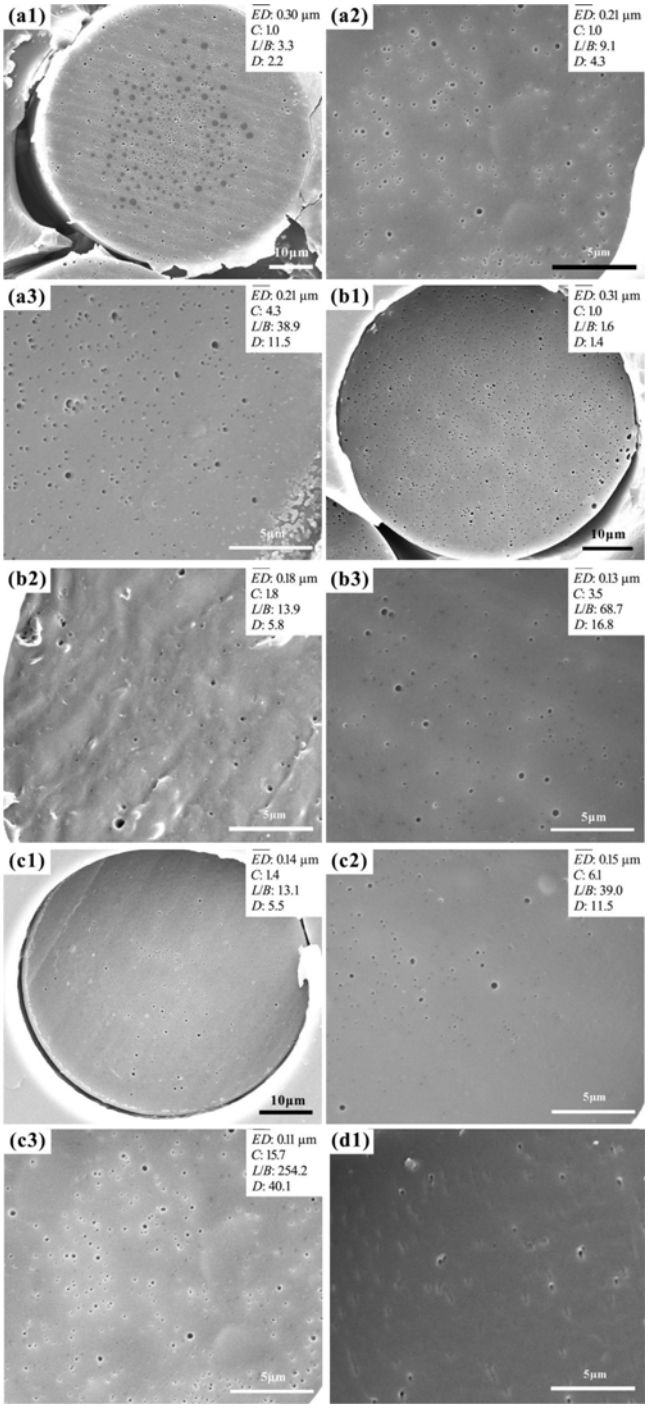

Figure 6. SEM micrographs of cross sections of fibers taken at (1) 250, (2) 500 and (3) 1000 m/min: (a) iPP/PS31, (b) iPP/PS46, (c) iPP/PS2, and (d) iPP/PS3.

$$D = \frac{L}{d_0} = C^{2/3}\left(\frac{\overline{ED}_{Ex}}{\overline{ED}_{v_L}}\right)^2 \tag{6}$$

where *L* and *B* were the length of major axis and minor axis of fibrils in ellipsoid respectively, d_0 diameter of the

Table 2. Image analysis results of iPP/aPS take-up fibers

v_L(m/min)		125	250	375	500	750	1000
$\overline{ED}$ (μm)	iPP/PS1	1.45	0.98	0.90	0.94	1.13	1.30
	iPP/PS31	0.40	0.30	0.25	0.21	0.23	0.21
	iPP/PS46	0.36	0.31	0.32	0.18	0.14	0.13
	iPP/PS2	0.27	0.14	0.13	0.15	0.11	0.11
	iPP/PS3	0.11	-	-	-	-	-
$\overline{n}$	iPP/PS1	234	185	151	79	61	20
	iPP/PS31	453	443	445	447	157	107
	iPP/PS46	670	668	648	364	242	191
	iPP/PS2	1449	1073	374	242	93	94
	iPP/PS3	267	-	-	-	-	-
C	iPP/PS1	1.3	1.7	2.1	4.0	5.1	15.6
	iPP/PS31	1.0	1.0	1.0	1.0	2.9	4.3
	iPP/PS46	1.0	1.0	1.0	1.8	2.8	3.5
	iPP/PS2	1.0	1.4	3.9	6.1	15.9	15.7
	iPP/PS3	7.8	-	-	-	-	-
L/B	iPP/PS1	18.1	74.1	116.0	199.7	148.1	295.1
	iPP/PS31	1.3	3.3	5.5	9.1	19.4	38.9
	iPP/PS46	1.0	1.6	1.5	13.9	43.7	68.7
	iPP/PS2	1.2	13.1	46.1	39.0	294.3	254.2
	iPP/PS3	129.9	-	-	-	-	-
D	iPP/PS1	6.9	17.6	23.8	34.2	28.0	44.3
	iPP/PS31	1.2	2.2	3.1	4.3	7.2	11.5
	iPP/PS46	1.0	1.4	1.3	5.8	12.4	16.8
	iPP/PS2	1.1	5.5	12.9	11.5	44.2	40.1
	iPP/PS3	25.6	-	-	-	-	-

spherical droplet with equal volume to the ellipsoidal fibril in take-up fibers, $\overline{ED}_{Ex}$ and $\overline{ED}_{v_L}$ average equivalent diameters of droplets in extrudate fibers and that of fibrils in take-up fibers respectively. The deformation ratio *D* was regarded as the extension ratio of droplet to fibril with consideration of the occurrence of coalescence.

From the morphology analysis, droplets coalesced mostly in take-up fibers, especially in high take-up velocities of iPP/PS1 and iPP/PS2, such as 750 and 1000 m/min, at which quantities of fibrils reduced drastically. This was attributed to flow induced coalescence which Fortelný [32] had analyzed. Coalescence was a consequence of droplet collisions brought on due to velocity difference. While droplets approached each other, their hydrodynamic interaction increased. When the droplets were closed enough, droplet deformation due to the axial force and the removal of the trapped continuous phase started, and the remainder of continuous phase was thinned as a film. If the critical distance of the droplets was achieved, rupture of the film occurred. An initial contact of droplets was followed by evolution of rupture, and result the formation of a coalesced droplet. According to Janssen [33], the critical film thickness h_{crit}, at which a sudden rupture of the film and thus coalescence occur, was governed by van der Waals forces; for micrometer-sized drops with interfacial tension of 5×10^{-3} N/m, h_{crit} was about 5 nm. As Figure 7 shown, the diameters of matrix fibers decreased as take-up velocities increased, and fibrils in such confined matrixes closed to each other in radial directions, and an increase of the collision probability between the neighboring droplet pairs was considered.

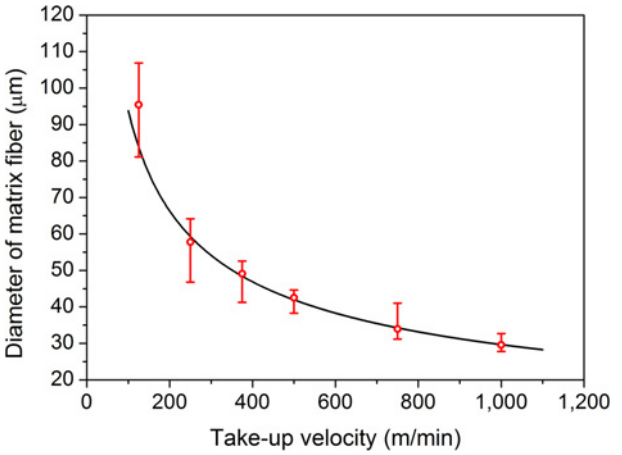

Figure 7. Diameter of matrix fiber as a function of take-up velocity: Comparison with experimental data (open cycle) and mass-conservation model (solid line).

As shown in Table 2, an increase of both *L*/*B* and *D* with the increase of take-up velocity from low to moderate one was found in all polymer pairs, while a slight decline was found in some polymer pairs (such as iPP/PS1 and iPP/PS2) at high velocity (such as 750 m/min). This was partially attributed to a monotonically increased gradient of velocity (or transient elongational strain rate) and thus a monotonically increased transient elongational stress with the increase of take-up velocity, which extended the spherical droplets to ellipsoidal fibrils. On the other hand, the coalescence discouraged the extension of the spherical droplets to ellipsoidal fibrils. When droplets coalesced, the droplets became larger in diameters, and the interfacial stresses (defined as interfacial tensions divided by radii) between matrices and droplets increased, thus fibrils trended to retracted to spheres. As shown in Table 2, high viscosity ratio trended to lead high *L*/*B* and *D*, while very low *L*/*B* and *D* were found in iPP/PS31 and iPP/PS46 relative to iPP/PS1 and iPP/PS2. These maybe due to PS31 and PS46 experienced different thermal history. PS31and PS46 were pre-blended by PS1 and PS2 prior to blended with iPP, while other aPS did not.

For the effect of take-up velocity on the size and quantity of fibrils in take-up fibers, fibrils in iPP/PS1 became finer as take-up velocity increased to 375 m/min, and then coarser while take-up velocity increased further more. For other iPP/aPS, fibrils showed a tendency to become finer as take-up velocity increased. For all iPP/aPS except iPP/PS3, fibrils

lessened as take-up velocity increased.

For iPP/PS3, composite fibers were prepared at all take-up velocities and morphologies on cross sections were observed as same as other composite fibers. Unfortunately, with current described analysis technology, MFM was observed only at 125 m/min. As Figure 6. d1 shown, only some concave surfaces were observed at higher take-up velocities, such as 250 m/min.

Prediction of Matrix-fibril Morphologies

During the melt spinning, the aPS droplets were stretched to fibrils by spin line tensile stresses, and squeezed to close to each other as matrix fibers cooled and solidified. The droplet deformation, breakup and coalescence played critical roles in MFM formation. Taking iPP/PS1 as an instance, the deformation and breakup of droplet in spin line were discussed in as follows.

Taylor was a pioneer in discussion the behavior of a fluid drop in shear flow, when the effects of fluid viscosity and interfacial tension were taken into account. Using the perturbation method with spherical shape as a zero approximation, Taylor [34] calculated the droplet deformation D in steady uniform shear flow and obtained first-order solutions. Cox [35] derived the equation for D in the steady uniaxial elongational flow as:

$$D = \frac{3}{2} \cdot Ca \cdot \frac{19p+16}{16p+16} \tag{7}$$

According to Huneault *et al.* [36], the deformation and breakup of droplets depended on the reduced capillary number Ca^*, which was the ratio of Ca to Ca_{crit}. In the case of Ca^* between 1 and 4, the droplet extended modestly in elongational flow until breakup occurred. The capillary number, Ca, signifying the competition of hydrodynamic stress to interfacial stress, was defined as below:

$$Ca = \frac{\text{hydrodynamic stress}}{\text{interfacial stress}} = \frac{\eta_m \dot{\gamma} R}{\sigma} \tag{8}$$

where η_m was the viscosity of matrix, $\dot{\gamma}$ the strain rate, R the radius of the undeformed droplet, and σ the interfacial tension. The critical capillary number, Ca_{crit}, was the critical value of the Ca at which droplet breakup may undergo. In elongational flow, Utracki *et al.* [37] suggested an empirical equation based on Grace's data [38] for the dependence of Ca_{crit} on p:

$$\lg(Ca_{crit}) = -0.64853 - 0.02442\lg p + 0.02221(\lg p)^2 - \frac{0.00056}{\lg p - 0.00645} \tag{9}$$

The average elongational strain rate of iPP/PS1 from exit of spinneret to solidification point was calculated from:

$$\bar{\dot{\varepsilon}} = \frac{v_L - v_0}{L_k} \tag{10}$$

where v_0 was the inertial velocity melt exited from spinneret, L_k the length of spin line from spinneret to solidification point, which was given based on steady-state melt spinning theory [39,40]:

$$L_k = \frac{WC_p}{\pi \bar{d}\bar{h}} \ln \frac{T_0 - T_a}{T_s - T_a} \tag{11}$$

where W was mass throughput of the matrix polymer, C_p the specific heat capacity of the matrix polymer, $\bar{d}$ the average diameter of the matrix fiber, $\bar{h}$ the average heat transfer coefficient from the fiber surface to the surrounding air, T temperature with subscript 0 of the spinneret, a of the quench air and s of the solidification point of the matrix polymer. $\bar{h}$ was calculated by [41]:

$$\bar{h} = 0.317\bar{d}^{-0.66}(\bar{v}^2 + 1024v_a^2)^{0.17} \tag{12}$$

where $\bar{v}$ was the average velocity, $\bar{v}=(v_0+v_L)/2$, and v_a was the cross air velocity.

The average elongation viscosities of the matrixes and the droplets were estimated by the Trouton's rule and the Arrhenius equation at $(T_0+T_s)/2$ with using the results of rheological properties discussed in the preceding section. The average capillary numbers and the critical capillary numbers were calculated by equation (8) and (9) respectively. And the average reduced capillary numbers were calculated

Table 3. Some estimated parameters in spin line of iPP/PS1 at various take-up velocities

v_L (m/min)	125	250	375	500	750	1000
L_k (m)	0.27	0.35	0.40	0.44	0.48	0.50
$\bar{\dot{\varepsilon}}$ (s^{-1})	7.0	11.3	15.1	18.7	25.8	32.7
$\overline{Ca}$	5.5	8.9	12.0	14.9	20.5	26.0
$\overline{Ca}^*$	23.6	38.0	50.9	63.2	87.2	110.6

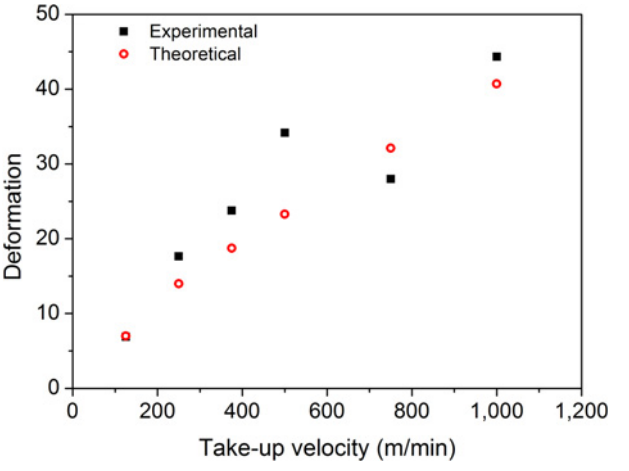

Figure 8. Comparison of experimental and theoretical average deformation ratio of droplet in iPP/PS1 take-up fibers.

by definitional equations. And then, the deformation of droplets was estimated by equation (7) in theoretically. The estimated results were summarized in Table 3 and plotted in Figure 8.

From the estimated results, at all velocities, $\overline{Ca}^*$ were larger than the critical value of 4. On an average view, a low probability of breakup of droplets was considered. In general, the elongational strain rate in melt spinning increases from a low plus value near to zero to a maximum and then decreases to zero at the solidification point. Only a very low elongational strain rate close to spinneret can lead to a very low *Ca* and a Ca^* of less than 4, and therefore the occurrence of droplet breakup. As shown in Figure 8, theoretical and experimental average deformation of droplets fitted very well at 125 m/min, while with the accuracy more than 80 % at velocities except 500 m/min. The accuracy was evaluated by

$$A = \left(1 - \left|\frac{D_{th}}{D_{ex}} - 1\right|\right) \times 100\% \quad (13)$$

where A was the accuracy, D the deformation ratios with subscripts "*th*" for theoretical data and "*ex*" for experimental ones. The difference of experimental and theoretical data was considered as be attributed to the observed severe coalescence. When the coalescence occurred, migrations of droplets to approach to each other and collisions of droplets were obvious, which led to energy dissipation, and a decrease of the actual deformation of droplets. Meanwhile, the deviations between theoretical and experimental values at velocity higher than 125 m/min hint the uncertainties of Newtonian fluids simplification at high take-up velocity.

Conclusion

Five melt-spun composite fibers were prepared by using iPP/aPS blends, and their morphologies were observed by SEM. It is found that spherical dispersed aPS phases appeared in extrudate composite fibers, and the diameters and quantities of aPS droplets depended strongly on the viscosity ratios of the blends. It is further observed that with the increase of the viscosity ratio, an exponential increase in diameters and an exponential decrease in quantities. Meanwhile, the effects of the viscosity ratios and take-up velocities on the size and quantities of aPS fibrils in take-up composite fibers were discussed, and it is noted that an increase of viscosity ratios led to increases of L/B and D of aPS fibrils, Moreover, a significant decrease in quantity of fibrils owing to severe coalescence occurred when the take-up velocity exceeded 500 m/min. Therefore, a relatively high viscosity ratio and a moderate take-up velocity would be expected to obtain aPS fibrils in high L/B and quantities.

Furthermore, a theoretical analysis based on the deformation theory was presented for predicting the deformation and breakup of droplets during melt spinning. A good fit between theoretical and observed experimental results was obtained at most discussed take-up velocities. The uncertainties of Newtonian fluids simplification and a hypothesis of local energy dissipation from migration and coalescence were noted to explain the deviations between the theoretical and experimental results.

Acknowledgments

The authors thank the National Natural Science Foundation of China (50903013), the Fundamental Research Funds for the Central Universities (12D10610 and 13D110614) and the National Natural Science Foundation for Distinguished Young Scholar of China (50925312) for financial support.

References

1. B. Favis and N. Chapleau, *J. Mater. Sci.*, **30**, 142 (1995).
2. J. Yang, J. L. White, and Q. Jiang, *Polym. Eng. Sci.*, **50**, 1969 (2010).
3. K. Friedrich, M. Evstatiev, S. Fakirov, O. Evstatiev, M. Ishii, and M. Harrass, *Compos. Sci. Technol.*, **65**, 107 (2005).
4. K. Jayanarayanan, S. Thomas, and K. Joseph, *J. Polym. Res.*, **18**, 1 (2011).
5. X. He, M. S. Ellison, and R. P. Paradkar, *J. Appl. Polym. Sci.*, **86**, 795 (2002).
6. H. Wang, X. Tao, E. Newton, and T. S. Chung, *Polym. J.*, **34**, 575 (2002).
7. J. Y. Kim, S. H. Kim, and T. Kikutani, *J. Polym. Sci. Polym. Phys.*, **42**, 395 (2004).
8. S. Y. Kim, S. H. Kim, S. H. Lee, and J. R. Youn, *Compos. Part A-Appl. S.*, **40**, 607 (2009).
9. R. McCardle, D. Bhattacharyya, and S. Fakirov, *Macromol. Mater. Eng.*, **297**, 711 (2012).
10. S. Sombatdee, T. Amornsakchai, and S. Saikrasun, *J. Polym. Res.*, **19**, 9843 (2012).
11. M. Afshari, R. Kotek, M. Haghighat Kish, H. Nazock Dast, and B. S. Gupta, *Polymer*, **43**, 1331 (2002).
12. M. Afshari, R. Kotek, B. S. Gupta, M. H. Kish, and H. N. Dast, *J. Appl. Polym. Sci.*, **97**, 532 (2005).
13. T. Takahashi, A. Konda, and Y. Shimizu, *Sen-I Gakkaishi*, **50**, 248 (1994).
14. A. Ujhelyiová, E. Bolhová, A. Marcinčin, and R. Tiňo, *Fiber Text. East. Eur.*, **15**, 26 (2007).
15. M. A. Tavanaie, A. M. Shoushtari, and F. Goharpey, *J. Macromol. Sci. Phys.*, **49**, 163 (2010).
16. C. Yu, M. Zhu, X. Shong, and Y. Chen, *J. Appl. Polym. Sci.*, **82**, 3172 (2001).
17. Q. Xing, M. Zhu, Y. Wang, Y. Chen, Y. Zhang, J. Pionteck, and H. J. Adler, *Polymer*, **46**, 5406 (2005).
18. N. A. Shitov, G. I. Timofeeva, and E. M. Aizenshtein, *Fibre Chem.*, **17**, 305 (1986).
19. Y. Qin, D. L. Brydon, R. R. Mather, and R. H. Wardman, *Polymer*, **34**, 1196 (1993).

20. Y. Qin, D. L. Brydon, R. R. Mather, and R. H. Wardman, *Polymer*, **34**, 1202 (1993).
21. Y. Qin, D. L. Brydon, R. R. Mather, and R. H. Wardman, *Polymer*, **34**, 3597 (1993).
22. T. Takahashi, A. Konda, and Y. Shimizu, *Sen-I Gakkaishi*, **52**, 507 (1996).
23. M. Afshari, R. Kotek, M. Haghighat Kish, H. Nazock Dast, and B. S. Gupta, *Polymer*, **43**, 1331 (2002).
24. A. D. Padsalgikar and M. S. Ellison, *Polym. Eng. Sci.*, **37**, 994 (1997).
25. C. H. Song and A. I. Isayev, *Polymer*, **42**, 2611 (2001).
26. Z. Pan, M. Zhu, Y. Chen, L. Chen, B. Sun, H. Yu, C. Jiang, and Z. Xu, *Fiber. Polym.*, **11**, 249 (2010).
27. Z. Pan, Y. Chen, M. Zhu, C. Jiang, Z. Xu, W. Lu, and J. Pionteck, *Fiber. Polym.*, **11**, 625 (2010).
28. Z. Pan, M. Zhu, Y. Chen, L. Chen, W. Wu, C. Yu, Z. Xu, and L. Cheng, *Fiber. Polym.*, **11**, 494 (2010).
29. A. R. Spurr, *J. Ultrastruct. Res.*, **26**, 31 (1969).
30. C. J. S. Petrie, *J. Non-Newton Fluid*, **137**, 15 (2006).
31. R. B. Bird and O. Hassager, "Dynamics of Polymeric Liquids: Fluid Mechanics", Wiley-Interscience, New York, 1987.
32. I. Fortelný in "Micro- and Nanostructured Multiphase Polymer Blend Systems Phase Morphology and Interfaces" (C. Harrats, S. Thomas, and G. Groeninckx Eds.), p.43, CRC Press, Boca Raton, 2006.
33. J. M. H. Janssen in "Materials Science and Technology" (H. E. H. Meijer Ed.), p.115, Wiley-VCH, Weinheim, Gennany, 1997.
34. G. I. Taylor, *Proc. R Soc. Lond A-Math. Phy.*, **146**, 501 (1934).
35. R. G. Cox, *J. Fluid Mech.*, **37**, 601 (1969).
36. M. A. Huneault, Z. H. Shi, and L. A. Utracki, *Polym. Eng. Sci.*, **35**, 115 (1995).
37. L. A. Utracki and Z. H. Shi, *Polym. Eng. Sci.*, **32**, 1824 (1992).
38. H. P. Grace, *Chem. Eng. Commun.*, **14**, 225 (1982).
39. R. Beyreuther and H. Brünig, "Dynamics of Fibre Formation and Processing: Modelling and Application in Fibre and Textile Industry", p.12, Springer, 2007.
40. A. Ziabicki in "Man-made Fibers: Science and Technology", (H. F. Mark, S. M. Atlas, and E. Cernia Eds.), Vol. 1, p.169, Interscience, New York, 1967.
41. H. Brünig, R. Beyreuther, and H. Hofman, *Int. Fiber. J.*, **14**, 104 (1999).